

Formation Control

Methinks if I should kiss thee, no control
 Within the thrilling brain could keep afloat
 The subtle spirit.

Lord Alfred Tennyson (1809–1892)

In this chapter, we present a brief discussion of methods for continuous and impulsive formation control: Formation establishment, maintenance, and reconfiguration. Formation maintenance is a relatively long-duration activity compared to establishment or reconfiguration. Hence, it is imperative that the reference relative orbit for formation maintenance be chosen as close as possible to that supported by the physics of the perturbed relative motion problem. Otherwise, the fuel required for control will be prohibitive, since perturbations due to J_2 , drag, and solar radiation pressure are persistent. In this regard, as much of the non-periodic effects of the perturbations as practically possible must be accommodated into the reference trajectory, a task made easy by establishing either the proper mean or averaged differential orbital elements. It may be recalled that the averaged elements are obtained from the mean elements by including the orbit averaged effects of the short-periodic variations. As shown previously in Chapter 8, selection of the proper initial mean differential elements is also important to achieve naturally bounded formations, thus minimizing the need for control.

10.1 CONTINUOUS CONTROL

The commonly-used continuous feedback control methods are based on Control Lyapunov Functions (CLF) and the Linear Quadratic Regulator (LQR); both are discussed in Chapter 3. While the CLF method is applicable to linear as well as nonlinear models, as the name implies, the LQR is valid only for linear models. However, LQR-based designs may be applicable to nonlinear systems but the margin of stability is limited. A discussion of robust stabilization methods is beyond the scope of this book.

10.1.1 The CLF approach

In this section, the CLF approach – presented in Section 3.6 – is used in the context of formation maintenance or tracking a reference orbit. Let the

equations of motion be represented in terms of the CW equations, perturbed by unmodeled nonlinear effects denoted by \mathbf{N} :

$$\ddot{\mathbf{x}} = F_1 \mathbf{x} + F_2 \dot{\mathbf{x}} + \mathbf{N} + \mathbf{u} \quad (10.1)$$

where

$$F_1 = \begin{bmatrix} 3n_0^2 & 0 & 0 \\ 0 & 0 & 0 \\ 0 & 0 & -n_0^2 \end{bmatrix} \quad (10.2)$$

and

$$F_2 = \begin{bmatrix} 0 & 2n_0 & 0 \\ -2n_0 & 0 & 0 \\ 0 & 0 & 0 \end{bmatrix} \quad (10.3)$$

Note that F_2 is a skew-symmetric matrix. We will use a natural solution to the CW equations as \mathbf{x}_r , our reference solution to be tracked. The control effort required to track the CW solution will be nonzero in the steady state due to the fact that \mathbf{x}_r does not satisfy Eq. (10.1) exactly. Nevertheless, \mathbf{x}_r does satisfy the following equation:

$$\ddot{\mathbf{x}}_r = F_1 \mathbf{x}_r + F_2 \dot{\mathbf{x}}_r \quad (10.4)$$

and the tracking error, given by $\mathbf{e} = \mathbf{x} - \mathbf{x}_r$, satisfies

$$\ddot{\mathbf{e}} = F_1 \mathbf{e} + F_2 \dot{\mathbf{e}} + \mathbf{N} + \mathbf{u} \quad (10.5)$$

A simple quadratic test Lyapunov function of the form

$$V = \frac{n_0^2}{2} \mathbf{e}^T \mathbf{e} + \frac{1}{2} \dot{\mathbf{e}}^T \dot{\mathbf{e}} \quad (10.6)$$

is selected and its derivative is obtained as shown below:

$$\dot{V} = n_0^2 \dot{\mathbf{e}}^T \mathbf{e} + \mathbf{e}^T \ddot{\mathbf{e}} \quad (10.7)$$

Equation (10.5) can be substituted in Eq. (10.7) to eliminate $\ddot{\mathbf{e}}$. A choice for the control law which cancels the nonlinear effects and induces asymptotic closed-loop stability of the error dynamics is

$$\mathbf{u} = -(n_0^2 + F_1) \mathbf{e} - \mathbf{N} - k n_0 \dot{\mathbf{e}} \quad (10.8)$$

where k is a positive constant (it can also be a positive definite matrix), which can be selected to achieve a desired speed of response. Furthermore, the closed-loop system satisfies

$$\ddot{\mathbf{e}} = -n_0^2 \mathbf{e} - k n_0 \dot{\mathbf{e}} \quad (10.9)$$

Hence, the tracking error approaches zero, asymptotically, but the steady-state control input will be equal to $\mathbf{N}(\mathbf{x}_r)$. Note that F_2 does not appear in Eq. (10.8) due to its skew-symmetric property. A discussion of the merits of including F_2 in the control law for redundancy and robustness is beyond the scope of this book.

A better reference trajectory can be obtained by applying the nonlinearity correction to the PCO and GCO solutions [106] and including the effects of J_2 . However, the simplest and most effective approach to formation maintenance is via the no along-track drift condition. For the two-body problem this is just a condition on matching the energies of the satellites or their semimajor axes. For the J_2 problem, the required $\delta\bar{a}$ is given by Eq. (8.15). The CLF can be written as

$$V = \frac{1}{2}(\delta\bar{a} - \delta\bar{a}_d)^2 \quad (10.10)$$

where $\delta\bar{a}_d$ is the desired mean differential semimajor axis. The first derivative of the CLF is

$$\dot{V} = (\delta\bar{a} - \delta\bar{a}_d)(\delta\dot{\bar{a}} - \delta\dot{\bar{a}}_d) = (\delta\bar{a} - \delta\bar{a}_d)\dot{\bar{a}}_1 \quad (10.11)$$

where the subscripts 0 and 1 stand for the chief and the deputy, respectively. Furthermore, $\delta\bar{a}_d$ has been assumed to be constant and the chief is assumed to be non-maneuvering and acted upon only by the J_2 perturbation. An approximation is also introduced by the direct substitution of the derivative of the osculating semimajor axis of the deputy from Gauss' variational equations (2.107) in Eq. (10.11):

$$\dot{a} = \frac{2a^2 e \sin f}{h} u_x + \frac{2a^2 p}{hr} u_y \quad (10.12)$$

where u_x and u_y are, respectively, the radial and along-track control accelerations. This approximation is consistent with the $\mathcal{O}(J_2)$ approximation of the mean-to-osculating element transformation adopted in this book. Eq. (10.12) suggests that u_y is more effective in controlling a than does u_x , especially for orbits with very small eccentricities. Assuming the use of tangential acceleration only and neglecting the error due to the mean-to-osculating element conversion, a control law for achieving the desired objective of no along-track drift is obtained from Eq. (10.11) as

$$\frac{2a_1^2 p_1}{h_1 r_1} u_{y1} = -k(\delta a - \delta a_d) \quad (10.13)$$

where k is a positive constant. The along-track control law of Eq. (10.13) is expressed in the \mathcal{L}_1 frame of reference of the deputy. In a nonlinear \mathcal{I} frame simulation, this control has to be expressed in the \mathcal{I} frame by using the \mathcal{L}_1 - \mathcal{I} coordinate transformation matrix, similar to Eq. (4.99), resulting in

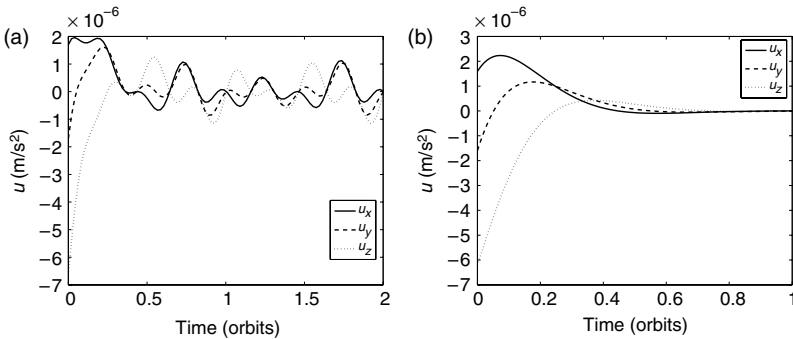


FIGURE 10.1 (a) ECI control components, osculating no along-track drift controller. (b) ECI control components, mean no along-track drift controller.

a control vector with three components. Furthermore, for practical application, the required instantaneous quantities such as a_0 , a_1 , p_1 , and h_1 can be calculated from the instantaneous position and velocity vectors of the two satellites. Such an implementation will be termed the *osculating element control law*. A simple modification of the above procedure by the use of \bar{a}_0 and \bar{a}_1 in the computation of $\delta\bar{a}$ results in the *mean element control law*. The advantage of using mean elements in the implementation of Eq. (10.13) is demonstrated on a simple example problem.

Example 10.1. Consider the following mean nonsingular orbital elements of the chief:

$$\begin{aligned} \bar{a}_0 &= 7100 \text{ km}, \bar{\theta}_0 = 0 \text{ rad}, \bar{i}_0 = 70^\circ \\ \bar{q}_{10} &= 0.01, \quad \bar{q}_{20} = 0, \quad \bar{\Omega}_0 = 45^\circ \end{aligned} \quad (10.14)$$

Assume that five of the six initial mean differential elements are in accordance with the PCO conditions, but the semimajor axis is arbitrarily chosen as $\delta a = 100 \text{ m}$, violating the no along-track drift condition.

The gain k is set equal to n_0 in Eq. (10.13). The \mathcal{I} frame components of the control histories are shown for the osculating and mean element controllers in Fig. 10.1(a) and Fig. 10.1(b), respectively. The initial transients in the controls seen in these figures are due to the error in $\delta\bar{a}$. The osculating element-based controls do not reach their steady states but show persistent activity; however, the mean element-based controls asymptotically approach zero within one orbit of the chief.

A discussion of the CLF approach to formation flying using Cartesian coordinates as well as orbital elements is provided in Ref. [29]. Sengupta and Vadali [31] use the CLF approach in conjunction with an Euler-parameter-based formation control law. De Queiroz *et al.* [165] present a CLF-based adaptive control technique for formation maintenance in the presence of uncertainties in the spacecraft masses and perturbations.

10.1.2 LQR control based on averaged orbital elements

Applications of the continuous-time LQR (cf. Section 3.7) to the CW model can be found in Refs. [154,166]. A direct application of the CW model-based control is inefficient for the J_2 problem since it does not account for the perturbed mean motion or quasi-periodic nature of the relative orbits [153, 156]. It has also been recognized that radial thrust is inefficient for formation maintenance near a circular orbit [152,167]. Fortunately, the CW model is controllable with only the along-track and cross-track control components.

In Section 8.7, we derived the modified CW equation, appropriate for modeling the formation maintenance problem. These equations are repeated again for ready reference:

$$\ddot{x} - 2\dot{\bar{M}}_0\dot{y} - 3\dot{\bar{M}}_0^2x = -3n_0^2x_{bias} + u_x \quad (10.15a)$$

$$\ddot{y} + 2\dot{\bar{M}}_0\dot{x} = u_y \quad (10.15b)$$

$$\ddot{z} + (\dot{\bar{M}}_0^2 + 2n_0\dot{\bar{\omega}}_0)z = -2\rho(0)kn_0 \sin \bar{i}_0^2 \sin \bar{\lambda}_0 \cos \alpha(0) + u_z \quad (10.15c)$$

The reference solutions selected in Section 8.7 are

$$\begin{aligned} x_r(t) &= 0.5 \left(1 + \frac{0.5\dot{\alpha}}{n_0} \right) \rho(0) \sin(\bar{\lambda}_0(0) + \alpha(0)) \\ &\quad + (\dot{\bar{M}}_0 + \dot{\alpha})t + x_{bias} \end{aligned} \quad (10.16a)$$

$$y_r(t) = \rho(0) \cos(\bar{\lambda}_0(0) + \alpha(0)) + (\dot{\bar{M}}_0 + \dot{\alpha})t \quad (10.16b)$$

$$z_r(t) = \rho(0) \sin(\bar{\lambda}_0(0) + \alpha(0)) + (\dot{\bar{M}}_0 + \dot{\alpha})t \quad (10.16c)$$

where x_{bias} is determined from Eq. (7.137) after substituting, respectively, for $\delta\bar{a}$ and $\delta\bar{i}$ from Eqs. (8.15) and (8.87) as

$$x_{bias} \approx -\frac{5}{4} J_2 \rho(0) \left(\frac{R_e}{\bar{a}_0} \right)^2 \sin(2\bar{i}_0) \cos \alpha(0) \quad (10.17)$$

The reference controls are

$$u_{x_r} = 0 \quad (10.18a)$$

$$u_{y_r} \approx -\rho(0)n_0\dot{\alpha} \cos(\bar{\lambda}_0(0) + \alpha(0)) + (\dot{\bar{M}}_0 + \dot{\alpha})t \quad (10.18b)$$

$$\begin{aligned} u_{z_r} &\approx 2n_0(\dot{\bar{\omega}}_0 - \dot{\alpha})\rho(0) \sin(\bar{\lambda}_0(0) + \alpha(0)) + (\dot{\bar{M}}_0 + \dot{\alpha})t \\ &\quad + 2\rho(0)kn_0 \sin^2 \bar{i}_0 \cos(\alpha(0)) \sin \bar{\lambda}_0 \end{aligned} \quad (10.18c)$$

The reference states and controls, respectively given by Eqs. (10.16a)–(10.16c) and Eqs. (10.18a)–(10.18c), also satisfy Eqs. (10.15). Hence the

six-dimensional error vector, $\mathbf{e} = \mathbf{x} - \mathbf{x}_r$, satisfies

$$\dot{\mathbf{e}} = A\mathbf{e} + B \begin{bmatrix} u_x \\ u_y - u_{y_r} \\ u_z - u_{z_r} \end{bmatrix} \quad (10.19)$$

where

$$A = \begin{bmatrix} 0 & 0 & 0 & 1 & 0 & 0 \\ 0 & 0 & 0 & 0 & 1 & 0 \\ 0 & 0 & 0 & 0 & 0 & 1 \\ 3\dot{\tilde{M}}_0^2 & 0 & 0 & 0 & 2\dot{\tilde{M}}_0 & 0 \\ 0 & 0 & 0 & -2\dot{\tilde{M}}_0 & 0 & 0 \\ 0 & 0 & -\dot{\tilde{M}}_0^2 - 2n_0\dot{\tilde{\omega}}_0 & 0 & 0 & 0 \end{bmatrix} \quad (10.20)$$

and

$$B = \begin{bmatrix} 0_{3 \times 3} \\ I_{3 \times 3} \end{bmatrix} \quad (10.21)$$

Thus, with the appropriate choices of Q and R , the LQR tracking control law for formation maintenance can be determined in terms of the error coordinates as

$$\mathbf{u} = -K\mathbf{e} \quad (10.22)$$

where K is the LQR gain matrix. There is no appreciable difference between the solutions for K with or without the term $2n_0\dot{\tilde{\omega}}_0 z$ included in Eq. (10.20). Similarly, the solution of the ARE is not significantly affected by replacing $\dot{\tilde{M}}_0$ in Eq. (10.20) by n_0 . Hence, K is based on the solution of the ARE for the CW model. The linear J_2 model presented in Section 7.5 has periodic coefficients and its use will require the gain matrix K to be periodic. Moreover, its state variables are influenced by the short-periodic variations in the differential orbital elements. In the implementation being discussed in this section the state variables are filtered by the averaging process of Section 7.4 and then used in the control law equation (10.22).

NUMERICAL RESULTS

Results of the application of the LQR for formation maintenance and fuel balancing without the use of radial thrust are presented in this section. We consider a formation of seven satellites in a 1 km, PCO configuration with initial phase angles ranging from 0° to 90° . The chief is assumed to be in a circular orbit with $\bar{a}_0 = 7100$ km. The control weight matrix is diagonal with the entries: $[1, 1]/n_0^4$; the state weight matrix is also diagonal with unit weights for the position errors and the rate error weights of n_0^{-2} for each axis. The simulation time period is 1500 orbits of the chief (equivalent to approximately 100 days). The $\dot{\alpha}$ value for each case considered is optimal for the selected inclination of the reference orbit.

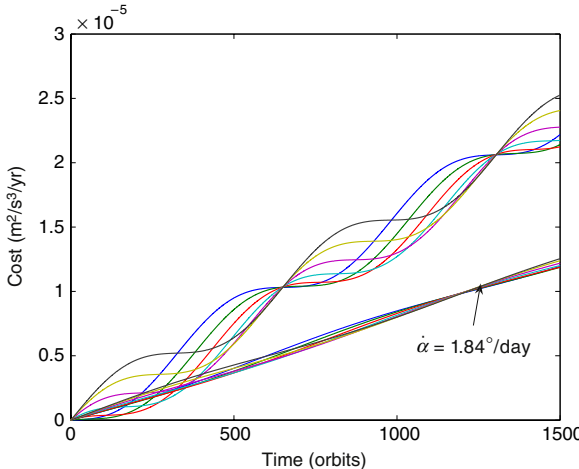


FIGURE 10.2 Cost vs. time with and without $\dot{\alpha}$, $i_0 = 49.11^\circ$, 1500 orbits.

Figure 10.2 shows, the individual satellite cost functions for $i_0 = 49.11^\circ$, obtained by evaluating Eq. (8.114) for each deputy and extrapolating the value over a period of one year. The variations of the costs for the satellites are shown for two cases, with and without fuel balancing. Each curve in this figure represents the cost for a single satellite. The fuel-balanced cost curves are close to each other and have a smaller average slope compared to the unbalanced cost curves. Hence, the average rate of fuel consumption with $\dot{\alpha} = 0$ is higher than that with $\dot{\alpha}_{opt} = 1.84^\circ/\text{day}$, the corresponding optimal rate. As can be seen from the figure, the use of the optimal rotation rate reduces the formation maintenance cost and simultaneously balances the inter-satellite fuel requirements to a great extent. Balancing the rate of fuel consumption results in the ballistic coefficients (cf. Section 1.3.4) of identical satellites remaining constant over the period of operation of the formation. This is important, since differential drag need not be considered as an additional perturbation in such a situation. The total formation maintenance cost (for seven satellites) with fuel balancing is $8.49 \times 10^{-5} \text{ m}^2/\text{s}^3/\text{year}$ compared to $1.59 \times 10^{-4} \text{ m}^2/\text{s}^3/\text{year}$, obtained by holding α constant for each satellite.

Figure 10.3 shows that, as discussed in Chapter 8, natural fuel balancing takes place for a formation with $i_0 = 54.73^\circ$ and $\dot{\alpha} = 0$, i.e., without any additional control induced formation rotation. The total formation maintenance cost for this case is $1.08 \times 10^{-4} \text{ m}^2/\text{s}^3/\text{year}$. This value of the inclination is ideal for fuel balancing, but not for the best fuel economy, since the out-of-plane formation maintenance cost increases with inclination. Figure 10.4 shows a cost comparison with and without fuel-balancing for $i_0 = 70^\circ$. The fuel balanced cost curves are very close to each other and can be easily distinguished from their counterparts. The optimal rotation-rate for this case is $\dot{\alpha}_{opt} = -4.1827^\circ/\text{day}$. The total cost with fuel balancing is $2.12 \times 10^{-4} \text{ m}^2/\text{s}^3/\text{year}$ compared to $5.56 \times 10^{-4} \text{ m}^2/\text{s}^3/\text{year}$, without.

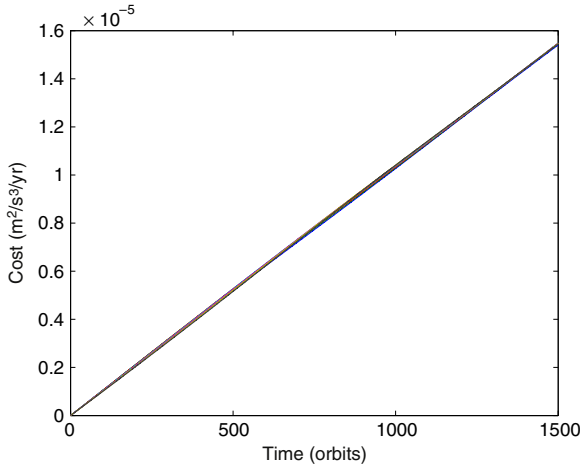


FIGURE 10.3 Cost vs. time with $\dot{\alpha} = 0$, $i_0 = 54.73^\circ$, 1500 orbits.

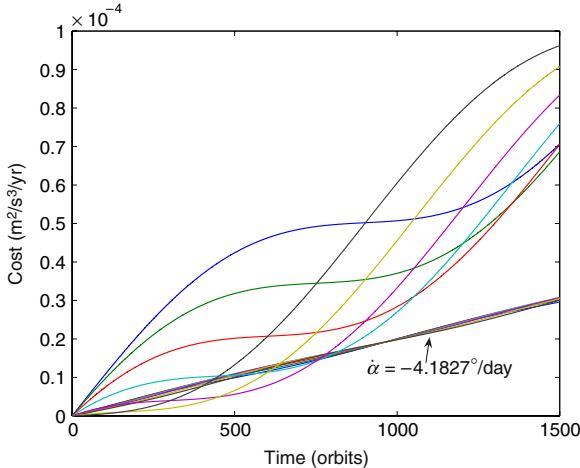


FIGURE 10.4 Cost vs. time with and without $\dot{\alpha}$, $i_0 = 70^\circ$, 1500 orbits.

These results show that longer-term extrapolations of fuel requirements for individual satellites, based on short-term simulations can be erroneous, especially when the individual costs are not well-balanced. However, it is reasonable to extrapolate the total fuel consumption for a PCO formation involving satellites with uniformly distributed initial phase angles over extended periods of time, since the process of cost-averaging virtually eliminates the periodic effects. Figures 10.2–10.4 show that the cost curves for the individual satellites have periodic variations, superimposed over their mean variations, for $\dot{\alpha} = 0$. The periodic components of the cost curves are relatively small compared to their respective linear growth terms when the fuel consumption is well-balanced.

Figures 10.5 and 10.6 show the plots of the along-track and cross-track components of the total and feedforward controls for a deputy with $\alpha(0) = 0$ and for

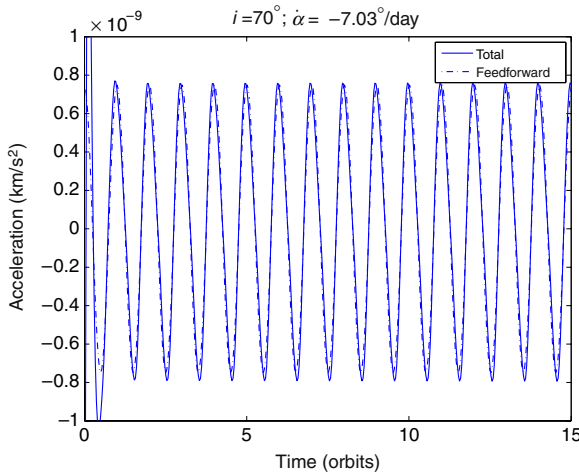


FIGURE 10.5 Comparison of the total and feedforward along-track controls.

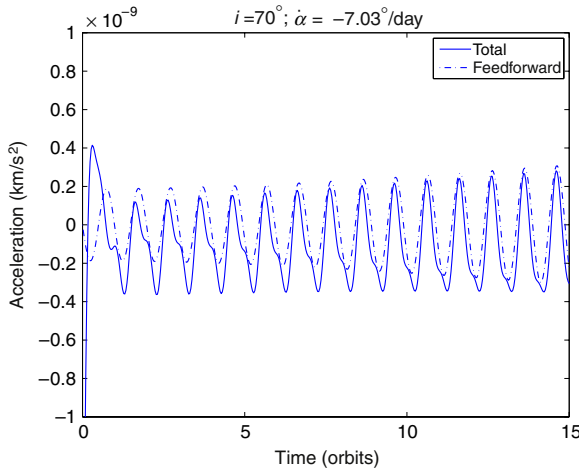


FIGURE 10.6 Comparison of the total and feedforward cross-track controls.

$i_0 = 70^\circ$ for a period of 15 orbits. The fundamental frequencies of the controls for each axis are the same. However, there is also a twice-per-orbit component in the total control which is not present in the feedforward, as can be ascertained from Fig. 10.7, which shows the differences between the two acceleration components for each axis. A small bias component is also visible in the cross-track acceleration error. These effects are caused by the short-periodic effects.

10.2 DISCRETE-TIME LQR CONTROL

The discrete-time LQR (DLQR) formulation, discussed in Section 3.7, is also applicable to the formation maintenance problem. Sherwood and Vassar [168] used the DLQR formulation with impulsive controls for the in-line formation

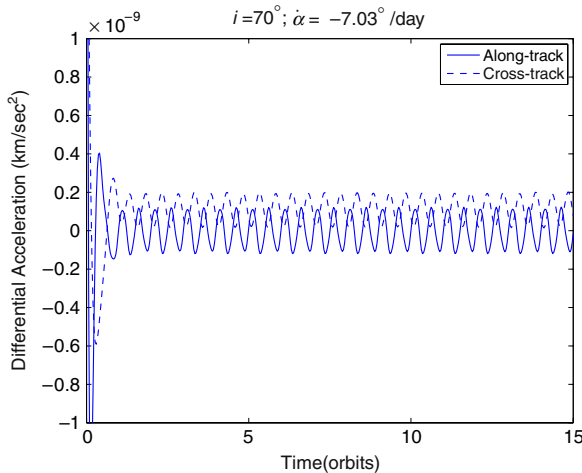


FIGURE 10.7 Differences between the total and feedforward accelerations.

maintenance of dissimilar satellites in a geostationary orbit, under the action of differential solar radiation pressure. The impulse application intervals for in-plane and out-of-plane corrections considered in this study are one and four hours, respectively. Ulybyshev [169] also presents such an application of the DLQR method for long-term formation keeping of a satellite constellation in LEO, using purely tangential maneuvers. We will treat the DLQR approach (cf. Section 3.7) with impulsive control in this section.

For the CW model, under the impulsive control assumption, the discrete-time state and control matrices are

$$A_d = e^{A \Delta T} \quad (10.23)$$

and

$$B_d = A_d B \quad (10.24)$$

where A and B are the state and control matrices for the CW equations and ΔT is the sample time (time between impulses). The reference solutions of Eqs. (10.16a)–(10.16c) do not satisfy the discrete-time model of the CW equations. There is a rigorous means of deriving the feedback gains for the tracking problem when the reference trajectories are known a priori. However, the implementation of such a control law requires a time-varying gain matrix. The results for the example problems treated in this section are based on the approximate control law of the form

$$\mathbf{u}(i) = -K(\mathbf{x}(i) - \mathbf{x}_r(i)) \quad (10.25)$$

with $\mathbf{x}_r(i)$, the reference trajectory, obtained by sampling Eqs. (10.16a)–(10.16c) at each sample time.

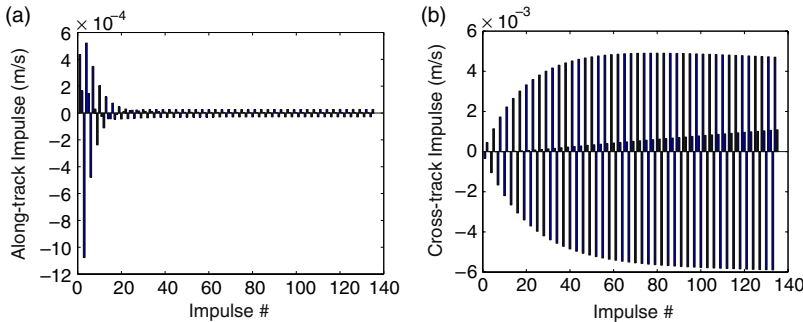


FIGURE 10.8 (a) Along-track impulses for $\dot{\alpha} = 0$. (b) Cross-track impulses for $\dot{\alpha} = 0$.

10.2.1 Numerical results

Results presented in this section are for the following mean nonsingular elements of the chief:

$$\begin{aligned}\bar{a}_0 &= 7100 \text{ km}, \quad \bar{\theta}_0 = 0 \text{ rad}, \quad \bar{i}_0 = 70^\circ \\ \bar{q}_{10} &= 0, \quad \bar{q}_{20} = 0, \quad \bar{\Omega}_0 = 0\end{aligned}\quad (10.26)$$

The initial conditions of the deputy are selected for a PCO with $\rho = 1$ km and $\alpha(0) = 0$. Two cases are considered: $\dot{\alpha} = 0$ and $\dot{\alpha} = -7.03^\circ/\text{day}$. The reference solution chosen for tracking is the same as that used for the continuous-time case. The state weight matrix Q is a diagonal matrix with entries 0.01 for the position errors and 0 for the velocity errors. The control weights for the two controls are n_0^{-2} . The simulations are carried out by integrating the nonlinear model. The integration process is stopped at each impulse application time and carried forward after the ECI velocity components of the deputy are updated by the impulses. The ECI components of the impulses are obtained from their LVLH counterparts given by Eq. (10.25). Figure 10.8 shows the along-track and cross-track impulse magnitudes for $\dot{\alpha} = 0$ for the case of three impulses per orbit, i.e., $\Delta T = \frac{2\pi}{3n_0}$. It is interesting to note that the along-track impulses rapidly decay after reaching a peak of approximately 6×10^{-4} m/s. The maximum cross-track impulse magnitude is 6×10^{-3} m/s. These figures show data for a duration of 3 days, too short for drawing any general conclusions regarding impulse magnitudes required for formation maintenance. Results for the second example, with $\dot{\alpha} = -7.03^\circ/\text{day}$, are shown in Fig. 10.9. Figure 10.9(a) shows a higher level of along-track impulse compared to that for the previous case and a reverse trend for the cross-track impulse due to the nonzero $\dot{\alpha}$. Simulations for a one-year period show that the cost for formation maintenance with $\dot{\alpha} = 0$ is 42.3 m/s/year and that for $\dot{\alpha} = -7.03^\circ/\text{day}$ is 36.5 m/s/year. No significant differences in the states or the impulse requirements were found with or without the use of the averaging filter.

These examples show the applications of the DLQR approach. However, the DLQR approach has a deficiency in that a large number of the impulses

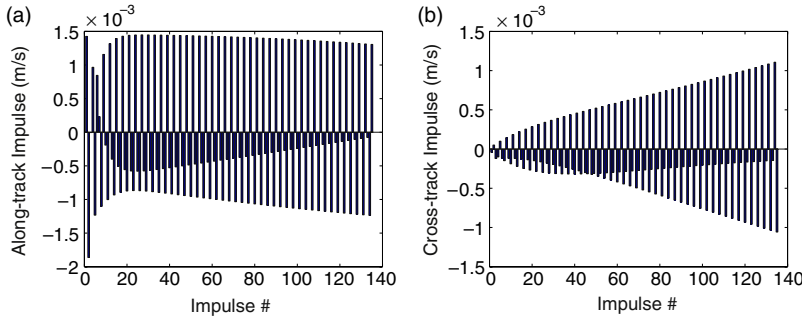


FIGURE 10.9 (a) Along-track impulses for $\dot{\alpha} = -7.03^\circ/\text{day}$. (b) Cross-track impulses for $\dot{\alpha} = -7.03^\circ/\text{day}$.

may be too small in magnitude for a practical implementation and the impulse application times are chosen a priori and not based on any optimality criterion. An alternative approach for formation maintenance with impulsive thrust is presented in the next section.

10.3 IMPULSIVE CONTROL BASED ON GAUSS' VARIATIONAL EQUATIONS

Gauss' variational equations (GVE), incorporating mean elements and the secular J_2 effects, offer a convenient model for computing solutions to multiple-impulse orbit transfer problems. This is so, because mean a , e , and i remain constant and the mean Ω , ω , and M vary linearly during the coasting phases. Approximate GVE for the mean classical orbital elements, including the effects of secular variations due to J_2 , are (cf. Eqs. (2.107) and Ref. [29])

$$\dot{\mathbf{e}} = \mathbf{A}(\mathbf{e}) + \mathbf{B}(\mathbf{e})\mathbf{u} \quad (10.27)$$

where $\mathbf{e} = [a \ e \ i \ \Omega \ \omega \ M]^T$, $\mathbf{u} = [u_x \ u_y \ u_z]^T$,

$$\mathbf{A}(\mathbf{e}) = \begin{bmatrix} 0 \\ 0 \\ 0 \\ -1.5J_2\left(\frac{R_e}{p}\right)^2 n \cos i \\ 0.75J_2\left(\frac{R_e}{p}\right)^2 n (5 \cos^2 i - 1) \\ n + 0.75J_2\sqrt{1-e^2}\left(\frac{R_e}{p}\right)^2 n (3 \cos^2 i - 1) \end{bmatrix} \quad (10.28)$$

and

$$B(\mathbf{e}) = \begin{bmatrix} \frac{2a^2 e \sin f}{h} & \frac{2a^2 p}{hr} & 0 \\ \frac{p \sin f}{h} & \frac{(p+r) \cos f + re}{h} & 0 \\ 0 & 0 & \frac{r \cos \theta}{r \sin \theta} \\ 0 & 0 & \frac{h}{r \sin i} \\ \frac{-p \cos f}{he} & \frac{(p+r) \sin f}{he} & \frac{-r \sin \theta \cos i}{h \sin i} \\ \frac{\eta(p \cos f - 2re)}{he} & \frac{-\eta(p+r) \sin f}{he} & 0 \end{bmatrix} \quad (10.29)$$

The true anomaly, f , is related to the mean anomaly through the following equations:

$$M = E - e \sin E \quad (10.30)$$

$$\tan \frac{f}{2} = \sqrt{\frac{1+e}{1-e}} \tan \frac{E}{2} \quad (10.31)$$

10.3.1 Formation establishment

The differential mean elements, δa , δe , and δi for each deputy, must be modified according to any one of the constraint criteria discussed in Chapter 8 to establish a formation. In addition, the mean $\delta \Omega$, $\delta \omega$, and δM must also satisfy certain shape and orientation requirements, such as those for PCO and GCO formations. The orbital elements undergo jump discontinuities at the impulse application times. During the coasting phases, they can be integrated analytically by using their mean secular rates. The true anomaly and the other time-varying quantities in the $B(\mathbf{e})$ matrix can be calculated by using the equations presented in Chapter 2. The impulse application times and the $\Delta \mathbf{v}$ magnitude/directions become the free parameters for optimization. Although the maximum number of impulses required for an optimal transfer is unknown a priori, it is not more than six, the number of orbital elements. Typically, 2–4 impulses are adequate for most orbit establishment maneuvers. Computation of a two-impulse maneuver requires the determination of six impulse components (three per impulse), the two impulse application times, and a final coast interval, leading to a total of nine parameters.

Two different performance measures can be constructed for the fuel-optimal transfer problem. If each impulse is assumed to be produced by a single thruster, with the capability for its pointing provided either by attitude control of the satellite or by a gimbal mechanism, then the performance index is

$$\mathcal{J}_1 = \sum_{j=1}^N \|\Delta \mathbf{v}_j\| = \sum_{j=1}^N \sqrt{\Delta v_{x_j}^2 + \Delta v_{y_j}^2 + \Delta v_{z_j}^2} \quad (10.32)$$

Special care must be taken for formulating the optimization problem for impulsive thrust maneuvers for the three-thruster case, since the fuel cost function is related to the absolute value of each impulse component. Following the approach of Ref. [170], which uses a procedure developed in the Linear Programming literature for the minimization of absolute value functions, each impulse magnitude is represented by two variables as follows:

$$\Delta v = \Delta v^+ - \Delta v^- \quad (10.33)$$

with Δv^+ and Δv^- bounded by

$$0 \leq \Delta v^+ \leq \Delta v_{max} \quad (10.34a)$$

$$0 \leq \Delta v^- \leq \Delta v_{max} \quad (10.34b)$$

where Δv_{max} is the maximum impulse magnitude. With the above representation, the performance index for an N-impulse maneuver can be written as

$$\mathcal{J}_2 = \sum_{j=1}^N (\Delta v_{x_j}^+ + \Delta v_{x_j}^- + \Delta v_{y_j}^+ + \Delta v_{y_j}^- + \Delta v_{z_j}^+ + \Delta v_{z_j}^-) \quad (10.35)$$

Note that either Δv^+ or Δv^- is always zero, resulting in \mathcal{J}_2 being the sum of the impulse magnitudes. Each component of an impulse can either be positive or negative, by virtue of Eqs. (10.33) and (10.34).

Example 10.2. Consider an example with the classical mean elements of the chief selected as

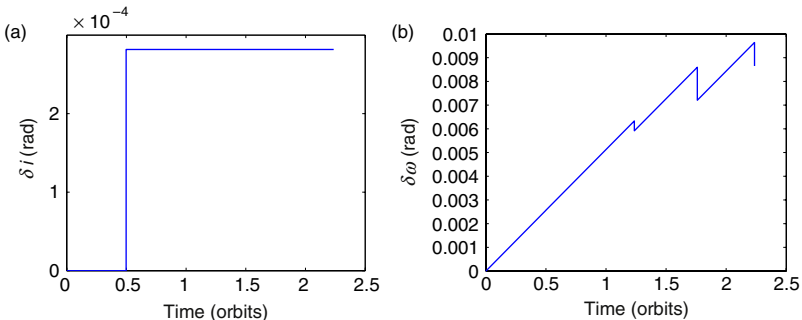
$$\mathbf{e}_0 = [7100 \text{ km } .05 \text{ } 48^\circ \text{ } 0 \text{ } 0 \text{ } 0]^T \quad (10.36)$$

The initial mean differential elements are all zero, except for $\delta \bar{M} = \rho / \bar{a}_0$, with $\rho_i = 1 \text{ km}$; indicating an in-line chief-deputy configuration with an initial separation of 1 km. The desired orbit element differences at the completion of the maneuver correspond to a PCO formation of $\rho_f = 2 \text{ km}$ and $\alpha = 0$, as given by Eqs. (8.83)–(8.87) and Eq. (8.15). The j th impulse application time is denoted by t_j . The time between the application of any two impulses is restricted to a maximum of one orbit. The optimal solutions obtained from the software package SNOPT [171] are presented in Table 10.1. The 2-impulse maneuver is carried out primarily by radial and cross-track thrust impulses; the along-track impulses required are much smaller. The impulses are separated by half the orbital period. Note that for the 2-impulse maneuver, $\mathcal{J}_1 < \mathcal{J}_2$ due to the triangle inequality. Estimates for circular orbits are $|\Delta v_{xy}| = \frac{1}{2} \rho_f n_0 = 1.05 \text{ m/s}$ for the in-plane impulse and $|\Delta v_z| = \rho_f n_0 = 2.1 \text{ m/s}$. These numbers match well with the data in Table 10.1.

It has been shown for continuous control, with three independent thrusters, that radial thrust is inefficient for formation maintenance. This assertion can be

Table 10.1 Impulse requirements for reconfiguration

	Δv_x m/s	Δv_y m/s	Δv_z m/s	Total m/s	t_j orbits
2-Imp	$\begin{bmatrix} 0.797 \\ -0.257 \end{bmatrix}$	$\begin{bmatrix} -0.002 \\ -0.002 \end{bmatrix}$	$\begin{bmatrix} 1.347 \\ -0.789 \end{bmatrix}$	$\mathcal{J}_1 = 2.395$	$\begin{bmatrix} 0 \\ 0.499 \end{bmatrix}$
2-Imp	$\begin{bmatrix} -0.257 \\ 0.796 \end{bmatrix}$	$\begin{bmatrix} -0.003 \\ 0 \end{bmatrix}$	$\begin{bmatrix} -2.008 \\ 0 \end{bmatrix}$	$\mathcal{J}_2 = 3.064$	$\begin{bmatrix} 0.5 \\ 1 \end{bmatrix}$
4-Imp	0	$\begin{bmatrix} 0 \\ -0.078 \\ 0.261 \\ -0.186 \end{bmatrix}$	$\begin{bmatrix} -2.008 \\ 0 \\ 0 \\ 0 \end{bmatrix}$	$\mathcal{J}_2 = 2.533$	$\begin{bmatrix} 0.498 \\ 1.236 \\ 1.76 \\ 2.236 \end{bmatrix}$

**FIGURE 10.10** (a) Change in δi . (b) Change in $\delta\omega$.

verified for maneuvers available with at least three impulses. For a 4-impulse maneuver performed with independent along-track and cross-track thrusters (no radial thrust), the number of free parameters are the eight impulse components, four impulse application times, and a final coast time. The results for this case are shown in the third row of Table 10.1. It is seen that there indeed is a reduction of the in-plane impulse by nearly 50% for the 4-impulse case. The example maneuver can also be performed with three impulses, but the required maneuver time will necessarily have to be longer in order to achieve the level of performance of the 4-impulse solution. Longer maneuver durations allow for the exploitation of the along-track drift caused by a differential semimajor axis. Figure 10.10(a) shows the variation in δi during the maneuver and the jump is a result of the cross-track impulse. On the other hand, Fig. 10.10(b) shows that $\delta\omega$ has secular growth as well as jump discontinuities. Finally, it is noted that for maneuvers performed over one or two orbits, the effect of J_2 is not significant and the impulse magnitudes and maneuver times can be well estimated by the two-body model.

Table 10.2 Impulse components and locations for a two-impulse reconfiguration scheme [3]

	First impulse	Second impulse
Orbit position	$\theta(t_1) = 2\pi - \alpha_i$	$\theta(t_2) = \theta(t_1) + \pi$
Radial	$-\frac{\sqrt{\delta q_1^2 + \delta q_2^2}}{2\gamma}$	$\frac{\sqrt{\delta q_1^2 + \delta q_2^2}}{2\gamma}$
Along-track	0	0
Cross-track	$\frac{\sqrt{\delta i^2 + \delta \Omega^2 \sin^2 i}}{\gamma}$	0

10.4 TWO-IMPULSE FORMATION RECONFIGURATION FOR CIRCULAR ORBITS

For impulse levels of the order of $\rho n_0 \times \mathcal{O}(J_2)$ and circular reference orbit s, the first-order approximations to Gauss' variational equations for the nonsingular elements introduced in Section 2.4, with $\lambda = M + \omega$ and $\theta = f + \omega$, are [3]:

$$\delta a \approx \frac{2}{n} \Delta v_y \quad (10.37a)$$

$$\delta \lambda \approx -2\gamma \Delta v_x - \gamma \sin \theta \cot i \Delta v_z \quad (10.37b)$$

$$\delta i \approx \gamma \cos \theta \Delta v_z \quad (10.37c)$$

$$\delta q_1 \approx \gamma \sin \theta \Delta v_x + 2\gamma \cos \theta \Delta v_y \quad (10.37d)$$

$$\delta q_2 \approx -\gamma \cos \theta \Delta v_x + 2\gamma \sin \theta \Delta v_y \quad (10.37e)$$

$$\delta \Omega \approx \frac{\gamma \sin \theta}{\sin i} \Delta v_z \quad (10.37f)$$

where Δv_x , Δv_y , and Δv_z are the magnitudes of the impulse components in the radial, tangential, and out-of-plane directions, respectively, and $\gamma = \sqrt{a/\mu}$. These equations form algebraic constraints for the formation reconfiguration and maintenance problems. As a matter of convenience, we drop the (\cdot) notation in this section while dealing with the mean elements.

Vaddi *et al.* [3] have developed a two-impulse scheme for formation establishment and reconfiguration based on Eqs. (10.37a)–(10.37f); their results are summarized in Table 10.2 in terms of the desired differential nonsingular elements, which can be obtained from Eqs. (10.41a)–(10.41e). In this scheme, the impulse application times for each satellite are determined by its initial phase angle α_i and they are separated in latitude angle by π . A single cross-track impulse and two equal and opposite radial impulses are applied for each satellite. Figure 10.11 shows two PCOs and the slot indicated by “1” shows the initial position of the deputy corresponding to $\alpha_i = 0$, when the chief is at the equator. Satellites from the inner PCO are to be reconfigured to the outer PCO and can be placed in any one of the slots indicated on the outer circle. The solution to the reconfiguration problem provides the fuel-optimal impulse magnitudes and the latitude angle of the chief at which they must be applied, and it performs the

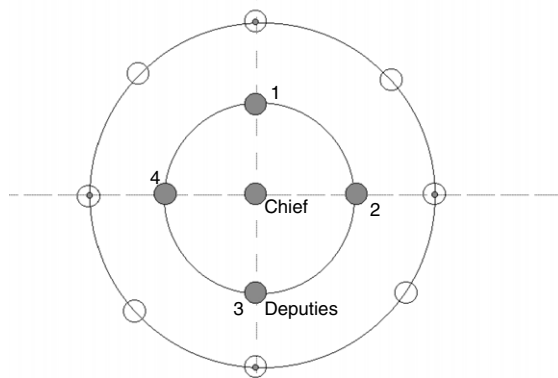


FIGURE 10.11 PCO-PCO reconfiguration (figure courtesy of S. Vaddi).

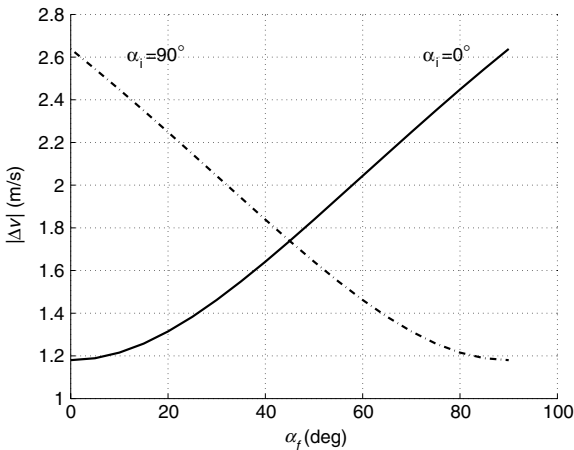


FIGURE 10.12 Impulse requirements for a PCO-PCO reconfiguration.

optimal slot selection process in the new PCO. For an example circular orbit of $a = 7100$ km and $i = 70^\circ$ and for reconfiguration from $\rho_i = 1$ km to $\rho_f = 2$ km, the impulse magnitudes are plotted as functions of the final phase angles for two satellites, with initial phase angles of 0 and 90° , in Fig. 10.12.

The cost curves for the two satellites show that the optimal solution for slot selection in the new PCO is to maintain the initial phase angle for each satellite. This result has also been derived by analysis in Ref. [3].

10.5 TWO-IMPULSE-PER-ORBIT FORMATION MAINTENANCE

A simpler, two-impulse-per-orbit feedback control scheme is presented in this section. This scheme does not require any iterative computation. The reference

solution chosen in this section is

$$x_r(t) = 0.5\rho \sin(\theta(t) + \alpha(t)) + \delta a \quad (10.38)$$

$$y_r(t) = \rho \cos(\theta(t) + \alpha(t)) \quad (10.39)$$

$$z_r(t) = \rho \sin(\theta(t) + \alpha(t)) \quad (10.40)$$

There is a difference in notation between Eqs. (10.38)–(10.40), which contain θ explicitly, and Eqs. (8.102)–(8.104), where $\dot{\omega}_0$ has effectively been absorbed into $\dot{\alpha}$. A procedure similar to that used for deriving Eqs. (8.83)–(8.87) leads to the following instantaneous differential mean elements, required to satisfy Eqs. (10.38)–(10.40):

$$\delta i(t) = \frac{\rho}{a_0} \cos \alpha(t) \quad (10.41a)$$

$$\delta q_1(t) = -\frac{\rho}{2a_0} \sin \alpha(t) \quad (10.41b)$$

$$\delta q_2(t) = -\frac{\rho}{2a_0} \cos \alpha(t) \quad (10.41c)$$

$$\delta \Omega(t) = -\frac{\rho}{a_0} \frac{\sin \alpha(t)}{\sin i_0} \quad (10.41d)$$

$$\delta \lambda(t) = -\delta \Omega(t) \cos i_0 \quad (10.41e)$$

The no along-track drift condition determines δa .

The desired mean differential elements at any instant t can be obtained by substituting in Eqs. (10.41a)–(10.41e) and Eq. (8.15), the instantaneous mean elements of the chief and

$$\alpha(t) = \alpha(0) + \dot{\alpha}t \quad (10.42)$$

The impulses required to produce the required changes in the elements of the deputies can be obtained from GVE.

10.5.1 Analytical solution for circular orbits

For a two-impulse-per-orbit control scheme, the impulse application times and the corresponding impulse vectors must be determined. If the impulse application times are known, then the problem boils down to the determination of six unknowns, which satisfy the six constraints imposed by Eqs. (10.37a)–(10.37f). Since the impulse application times are functions of α , which has inter-satellite as well as temporal variations, their direct, closed-form solutions are desirable. The approach presented for formation maintenance, although not necessarily optimal, offers a practical, non-iterative solution. It is an adaptation of the method proposed by Vaddi et al. [3] to the solution of the J_2 problem [4]. The principal assumption herein is the dominance of the out-of-plane impulse magnitude over that required for in-plane formation maintenance when

$\dot{a} \neq 0$. Additionally, the mean elements are substituted for osculating elements in Eqs. (10.37a)–(10.37f), since the theory is accurate to $\mathcal{O}(J_2)$.

The details of the formation maintenance constraints for an N -impulse control scheme can be obtained by incorporating the differential drift rates into Eqs. (10.37a)–(10.37f). It is noted from Eqs. (10.37a) and (10.37c) that δa and δi are piecewise-constant functions, with jumps at the impulse application points. On the other hand, $\delta\lambda$ and $\delta\Omega$ can have jumps as well as linear variation with respect to time. Each instant at which δi jumps due to an impulse, the drift rates, $\delta\dot{\lambda}$ and $\delta\dot{\Omega}$, also undergo changes, as given by Eq. (8.89a). The effect of perigee rotation of the chief influences the evolution of δq_1 and δq_2 . These details have been incorporated into the following constraint functions:

$$\delta a_d(t_f) - \delta a(t_0) = \frac{2}{n_0} \sum_{j=1}^N \Delta v_{y_j} \quad (10.43a)$$

$$\begin{aligned} \delta\lambda(t_f) - \delta\lambda(t_0) &= \Delta t_{f0} \left(\frac{\partial \dot{\lambda}}{\partial i} \delta i(t_0) + \frac{\partial \dot{\lambda}}{\partial a} \delta a(t_0) \right) \\ &\quad + \sum_{j=1}^N \left(-2\gamma \Delta v_{x_j} + \frac{2}{\gamma} \frac{\partial \dot{\lambda}}{\partial a} \Delta t_{fj} \Delta v_{y_j} \right. \\ &\quad \left. - \gamma \{ \cot i_0 \sin \theta_j - \frac{\partial \dot{\lambda}}{\partial i} \cos \theta_j \Delta t_{fj} \} \Delta v_{z_j} \right) \end{aligned} \quad (10.43b)$$

$$\delta i_d(t_f) - \delta i(t_0) = \gamma \sum_{j=1}^N \cos \theta_j \Delta v_{z_j} \quad (10.43c)$$

$$\begin{aligned} \begin{Bmatrix} \delta q_{1d}(t_f) \\ \delta q_{2d}(t_f) \end{Bmatrix} &- \begin{bmatrix} \cos(\dot{\omega} \Delta t_{f0}) & -\sin(\dot{\omega} \Delta t_{f0}) \\ \sin(\dot{\omega} \Delta t_{f0}) & \cos(\dot{\omega} \Delta t_{f0}) \end{bmatrix} \begin{Bmatrix} \delta q_1(t_0) \\ \delta q_2(t_0) \end{Bmatrix} \\ &= \gamma \sum_{j=1}^N \begin{bmatrix} \sin(\theta_j + \dot{\omega} \Delta t_{fj}) & 2 \cos(\theta_j + \dot{\omega} \Delta t_{fj}) \\ -\cos(\theta_j + \dot{\omega} \Delta t_{fj}) & 2 \sin(\theta_j + \dot{\omega} \Delta t_{fj}) \end{bmatrix} \begin{Bmatrix} \Delta v_{x_j} \\ \Delta v_{y_j} \end{Bmatrix} \end{aligned} \quad (10.43d)$$

$$\begin{aligned} \delta\Omega_d(t_f) - \delta\Omega(t_0) &= \Delta t_{f0} \frac{\partial \dot{\Omega}}{\partial i} \delta i(t_0) \\ &\quad + \gamma \sum_{j=1}^N \left(\frac{\partial \dot{\Omega}}{\partial i} \cos \theta_j \Delta t_{fj} + \frac{\sin \theta_j}{\sin i_0} \right) \Delta v_{z_j} \end{aligned} \quad (10.43e)$$

where $(.)_d$ indicates the desired differential orbital element, t_f is the final time, θ_j is the latitude angle at the instant of the j th impulse application, and $\Delta t_{kl} = t_k - t_l$. The coupling between the in-plane and out-of-plane dynamics is affected by the presence of Δv_z in Eq. (10.43b). Equations (10.43a)–(10.43e) can be applied for calculating the impulse magnitudes during each orbit.

Equations (10.43) can be simplified with the knowledge that the change in $\delta\Omega$ over an orbit, due to changes in δi , is small compared to that produced directly by the impulses. This approximation in Eq. (10.43e) results in the following equation for determining the two values of the latitude angle, separated by π , at

which it is ideal to perform the out-of-plane maneuvers for each satellite:

$$\tan \theta_{1,2} = \frac{\sin i_0 [\delta\Omega_d(t_f) - \delta\Omega(t_0) - \Delta t_{f0} \frac{\partial \dot{\Omega}}{\partial i} \delta i(t_0)]}{\delta i_d(t_f) - \delta i(t_0)} \quad (10.44)$$

The impulse magnitudes can also be solved for from the simplified forms of Eq. (10.43c) and Eq. (10.43e). The total impulse magnitude is distributed equally among the two impulses:

$$\begin{aligned} \Delta v_{z1,2} = & \\ \pm \frac{1}{2\gamma} \sqrt{\sin^2 i_0 [\delta\Omega_d(t_f) - \delta\Omega(t_0) - \Delta t_{f0} \frac{\partial \dot{\Omega}}{\partial i} \delta i(t_0)]^2 + [\delta i_d(t_f) - \delta i(t_0)]^2} & \end{aligned} \quad (10.45)$$

The solution obtained from Eq. (10.44) should be modulated to lie between 0° and 180° , if it is negative. If the solution is positive to begin with, then the positive sign applies for Δv_z obtained from Eq. (10.45), otherwise the negative sign should be chosen. Once the particulars for the first impulse are known, then the information regarding the second impulse can be obtained as $\theta_2 = \theta_1 + \pi$ and $\Delta v_{z2} = -\Delta v_{z1}$. This completes the process for determining the impulse application times and out-of-plane impulse magnitudes. Equations (10.44) and (10.45) are not accurate if the times between the impulses are long (more than 10–15 orbits), due to the approximation employed to derive them.

Knowing the two impulse application times, the remaining four equations (10.43a), (10.43b), and (10.43d) can be solved to obtain the four components of the two in-plane impulses. The only remaining question is how to determine an optimal value for $\dot{\alpha}$.

10.5.2 Determination of $\dot{\alpha}$ for fuel balancing

Equations (10.43) can be simplified by using the small-angle approximation, especially if the corrections are to be applied during each and every orbit. For such a case, the out-of-plane constraint equations are

$$-\frac{\rho}{a_0} \sin \alpha(0) \dot{\alpha} \Delta t_{f0} = \gamma \sum_{j=1}^N \cos \theta_j \Delta v_{zj} \quad (10.46a)$$

$$-\frac{\rho}{a_0} \cos \alpha(0) \left(\dot{\alpha} + \frac{\partial \dot{\Omega}}{\partial i} \sin i_0 \right) \Delta t_{f0} = \gamma \sum_{j=1}^N \sin \theta_j \Delta v_{zj} \quad (10.46b)$$

Since the two out-of-plane impulse magnitudes are equal, and as θ_1 and θ_2 are separated by 180° , Eqs. (10.46a) show that the total out-of-plane impulse magnitude per orbit is related to $\dot{\alpha}$ as shown below:

$$\Delta v_z = (\rho n_0) \Delta t_{f0} \sqrt{\sin^2 \alpha(0) \dot{\alpha}^2 + \cos^2 \alpha(0) \left(\dot{\alpha} + \frac{\partial \dot{\Omega}}{\partial i} \sin i_0 \right)^2} \quad (10.47)$$

Estimates of the impulse requirements are provided for a PCO with $\rho = 1$ km and a reference orbit with the following mean elements:

$$\begin{aligned} a_0 &= 7.092 \text{ km}, \quad \theta_0 = 0 \text{ rad}, \quad i_0 = 70^\circ \\ q_{10} &= 0, \quad q_{20} = 0, \quad \Omega_0 = 45^\circ \end{aligned} \quad (10.48)$$

The out-of-plane impulse obtained from Eq. (10.47) with $\alpha(0) = 0$ and $\dot{\alpha} = 0$ is 40.8 m/s/year. By substituting for $\frac{\partial \dot{\Omega}}{\partial i}$ from Eq. (8.90) and minimizing Eq. (10.47) with respect to $\dot{\alpha}$, we obtain

$$\dot{\alpha}_{Sat} = -\frac{\partial \dot{\Omega}}{\partial i} \sin i_0 \cos^2 \alpha(0) = -\frac{3}{2} J n_0 \sin^2 i_0 \cos^2 \alpha(0) \quad (10.49)$$

Equation (10.49) shows that $\dot{\alpha}$ is a function of $\alpha(0)$, and it is zero for $\alpha(0) = 90^\circ$. Furthermore, Eqs. (8.90c), (10.47) and (10.49) show that $\Delta v_z = 0$ for the satellite with $\alpha(0) = 0^\circ$, an obvious result, but of limited utility for formation fuel balancing. A more useful result is obtained by averaging the above expression over $\alpha(0) \in [0, 2\pi]$:

$$\dot{\alpha}_{Formation} = -\frac{1}{2} \frac{\partial \dot{\Omega}}{\partial i} \sin i_0 = -\frac{3}{4} J n_0 \sin^2 i_0 \quad (10.50)$$

Equation (10.50) can be substituted in Eq. (10.47) to obtain

$$\Delta v_{zav} = \pi \rho \frac{\partial \dot{\Omega}}{\partial i} \sin i_0 / \text{orbit/satellite} \quad (10.51)$$

An estimate of the average out-of-plane impulse requirement per-satellite-year, based on Eq. (10.51), is 20.3 m/s. A similar estimate is obtained if the out-of-plane impulse requirements are averaged for two satellites, with $\alpha(0) = 0$ and $\alpha(0) = 90^\circ$. Accounting for the difference in the definition of α between Eqs. (8.102)–(8.104) and Eqs. (10.38)–(10.40), it can be verified that the results of Eq. (8.118) and Eq. (10.50) are quite close to each other. Hence, the equivalent result for the optimal formation rotation rate consistent with Eqs. (10.38)–(10.40) is

$$\dot{\alpha}_{Formation}^* = -\frac{16}{17} \left(\frac{3}{4} J n_0 \sin^2 i_0 \right) - \frac{1}{17} \dot{\omega} \quad (10.52)$$

Application of Eq. (10.52) for the reference orbit data (10.48) results in $\dot{\alpha} = -2.723^\circ/\text{day}$.

10.5.3 In-plane thrust requirements

The approximations utilized for Eqs. (10.43c) and (10.43e) can also be applied to the remaining equations in (10.43) resulting in

$$\frac{7\rho}{2} J \dot{\alpha} \sin 2i_0 \sin \alpha(0) \Delta t_{f0} = \frac{2}{n_0} \sum_{j=1}^N \Delta v_{y_j} \quad (10.53a)$$

$$\frac{\rho}{a_0} \cos \alpha(0) (\dot{\alpha} \cot i_0 + \frac{3}{4} n_0 J \sin 2i_0) \Delta t_{f0} = \sum_{j=1}^N \left(-2\gamma \Delta v_{x_j} + \frac{2}{\gamma} \frac{\partial \dot{\lambda}}{\partial a} \Delta t_{fj} \Delta v_{y_j} - \gamma \left\{ \cot i_0 \sin \theta_j - \frac{\partial \dot{\lambda}}{\partial i} \cos \theta_j \Delta t_{fj} \right\} \Delta v_{z_j} \right) \quad (10.53b)$$

$$\begin{aligned} \frac{\rho}{2a_0} (\dot{\alpha} + \dot{\omega}) \Delta t_{f0} & \left\{ \begin{array}{c} -\cos \alpha(0) \\ \sin \alpha(0) \end{array} \right\} \\ & = \gamma \sum_{j=1}^N \begin{bmatrix} \sin(\theta_j + \dot{\omega} \Delta t_{fj}) & 2 \cos(\theta_j + \dot{\omega} \Delta t_{fj}) \\ -\cos(\theta_j + \dot{\omega} \Delta t_{fj}) & 2 \sin(\theta_j + \dot{\omega} \Delta t_{fj}) \end{bmatrix} \begin{Bmatrix} \Delta v_{x_j} \\ \Delta v_{y_j} \end{Bmatrix} \quad (10.53c) \end{aligned}$$

Equations (10.53) show the complex structure of the in-plane formation maintenance and fuel balancing problem. Equation (10.53a) shows that irrespective of the value of $\alpha(0)$, the sum of the tangential impulses must equal zero, for $\dot{\alpha} = 0$. Neglecting the terms containing Δt_{fj} in Eq. (10.53b), it is seen that the net radial impulse, for the most part, has to counter the effect of the out-of-plane impulses. The δq_1 and δq_2 equations (Eq. (10.53c)) show that the total in-plane impulse magnitude is bounded between the two values provided by the following equations:

$$\Delta v_x = \pi \rho (\dot{\omega} + \dot{\alpha}) \text{(Radial thrust only, per orbit)} \quad (10.54a)$$

$$\Delta v_y = \frac{1}{2} \pi \rho (\dot{\omega} + \dot{\alpha}) \text{(Tangential thrust only, per orbit)} \quad (10.54b)$$

For the reference orbit selected and with $\dot{\alpha} = 0$, the in-plane costs, considering eccentricity and perigee constraints, can vary between 2.5–5 m/s/year; the lower value applies for the case with tangential thrust only. The inefficiency of continuous radial thrust for this particular problem has been discussed in Ref. [139]. However, the two-impulse scheme does not allow for the luxury of not using radial thrust.

For the special case of $\alpha_0 = 90^\circ$ and $\dot{\alpha} = 0$, Eqs. (10.46) show that $\Delta v_z = 0$. Hence, the assumption of the dominance of Δv_z does not apply for this case. However, when $\dot{\alpha} \neq 0$, this assumption is quite reasonable.

NUMERICAL RESULTS

A formation of seven satellites in the PCO configuration is considered with $\rho = 1$ km. The initial phase angles range from 0° to 90° , in 15° increments. The mean elements of the reference orbit are given in Eq. (10.48). The total impulse requirements are computed by summing the 1-norm of the applied impulse vectors. Simulation results are shown for a period of one year and are obtained by integrating the nonlinear equations of motion of the individual satellites. The integration process is terminated just before the application of each impulse and restarted after updating the velocity of each satellite with the velocity increment. The \mathcal{L} -frame impulse vectors are transformed into their \mathcal{I} -frame components and then applied to update the velocity vectors of the satellites.

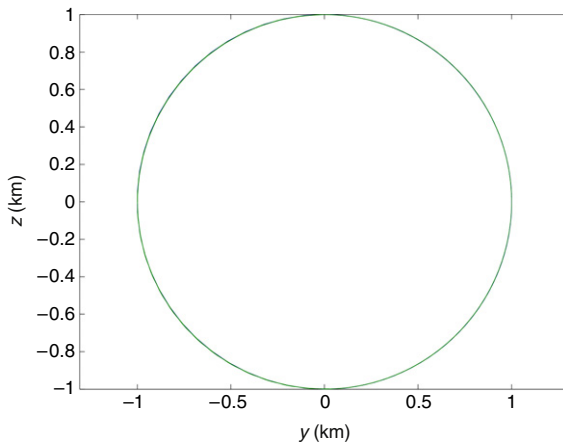


FIGURE 10.13 Resulting relative orbits for $\alpha(0) = 0$ due to the application of control, $\dot{\alpha} = 0$ (one-year simulation).

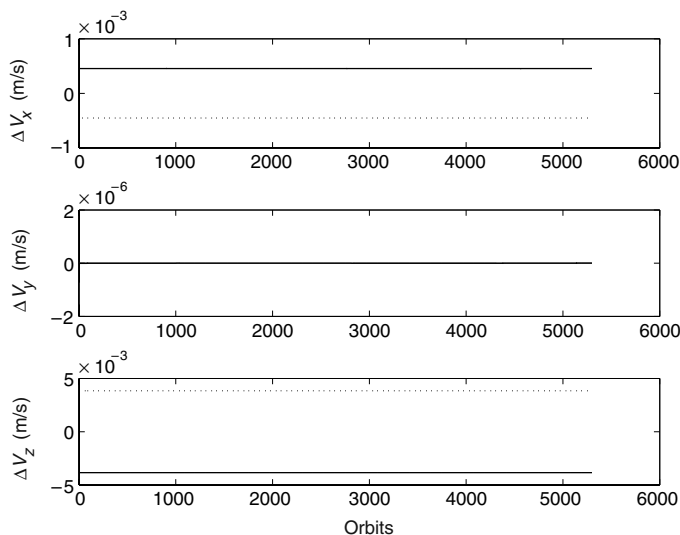


FIGURE 10.14 Impulse components required for controlling a satellite with $\alpha(0) = 0$ and $\dot{\alpha} = 0$.

The result of applying the two-impulse-per-orbit scheme on a satellite with $\alpha(0) = 0$ and $\dot{\alpha} = 0$ is shown in Fig. 10.13. This figure should be compared with the first of Fig. 8.21 to appreciate the effectiveness of the proposed control scheme. The deviation of the controlled PCO from its reference is within ± 1 m for each of the three coordinate axes. The required impulse magnitudes are shown in Fig. 10.14. The impulse magnitudes remain unchanged over time and are nearly the same for the two impulses during each orbit. The two impulse directions are opposite to each other. The out-of-plane impulse magnitudes are

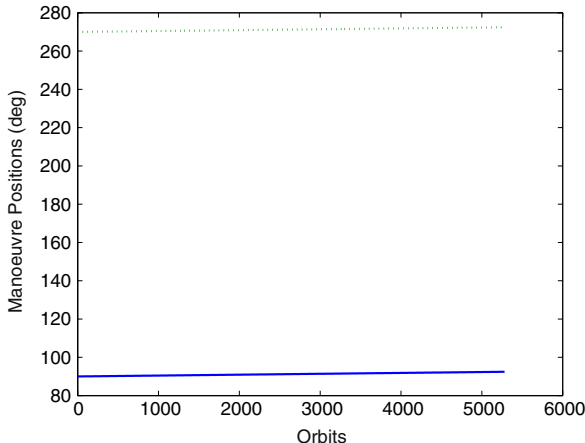


FIGURE 10.15 Impulse application points with respect to the chief's orbit for $\alpha(0) = 0$ and $\dot{\alpha} = 0$.

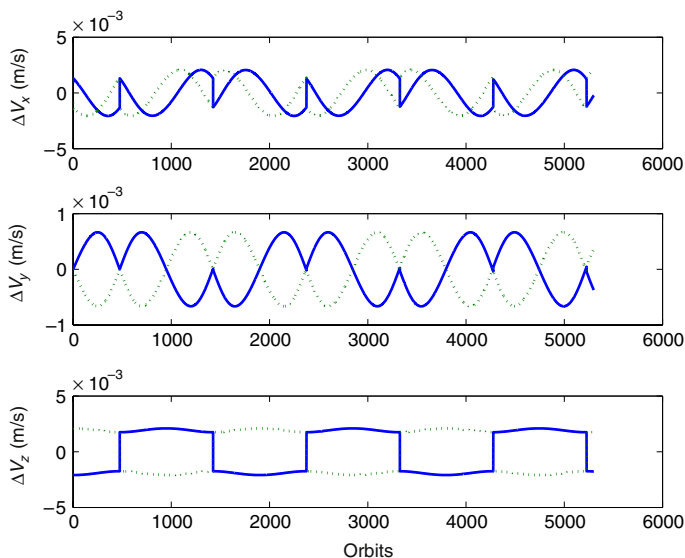


FIGURE 10.16 Impulse components for $\alpha(0) = 0$ and $\dot{\alpha} = -2.723^\circ/\text{day}$.

of the order of 4×10^{-3} m/s. The radial impulse magnitude is approximately 0.5×10^{-3} m/s and the tangential impulse is negligible when compared to the other two components. The impulse application instants are shown with respect to the latitude angle of the chief in Fig. 10.15 and they remain very nearly constant. The first impulse is applied at $\theta_1 \approx 90^\circ$ and the second at $\theta_2 \approx 270^\circ$.

The next set of results are for a satellite with $\alpha(0) = 0$ and $\dot{\alpha} = -2.723^\circ/\text{day}$, computed from Eq. (10.52). The impulse magnitudes undergo periodic changes as shown in Fig. 10.16. Note that the radial and out-of-plane impulse

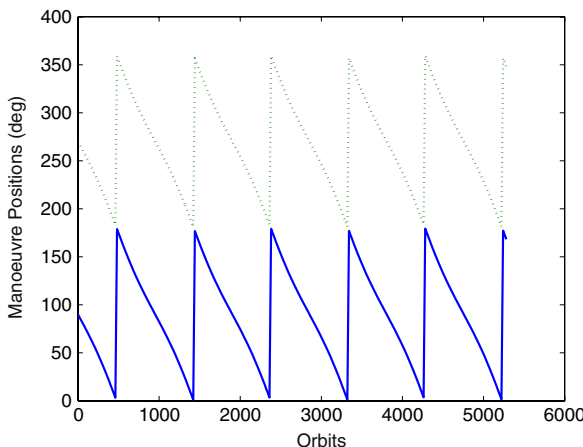


FIGURE 10.17 Impulse application points with respect to the chief's orbit for $\alpha(0) = 0$ and $\dot{\alpha} = -2.723^\circ/\text{day}$.

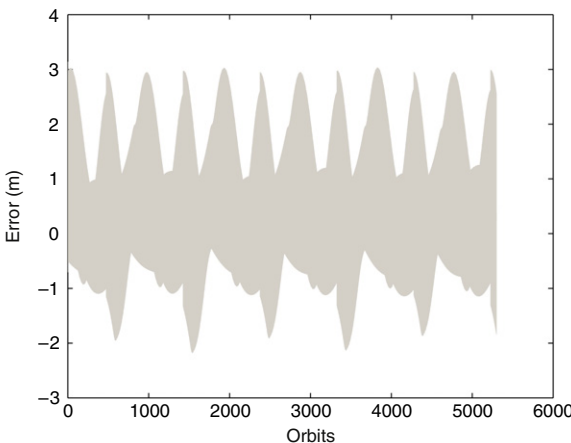


FIGURE 10.18 Evolution of the error in the radius of the PCO for $\alpha(0) = 0$ with the application of control, $\dot{\alpha} = -2.723^\circ/\text{day}$ (1 year).

components have the same extrema. There is a reduction in the maximum out-of-plane impulse magnitude, coupled with an increase in that for the radial component with respect to their levels shown in Fig. 10.14. The redistribution of the impulse levels, however, leads to a degree of sub-optimality in the control, since the derivation of the control law is based on the assumption that the cross-track impulse magnitude dominates that of the in-plane impulse. The impulse application points, shown in Fig. 10.17, vary between $0\text{--}180^\circ$ for the first impulse and $180\text{--}360^\circ$ for the second. The error in the radius of the PCO is limited to ± 3 m as indicated by Fig. 10.18. The reason for the apparent increase in the

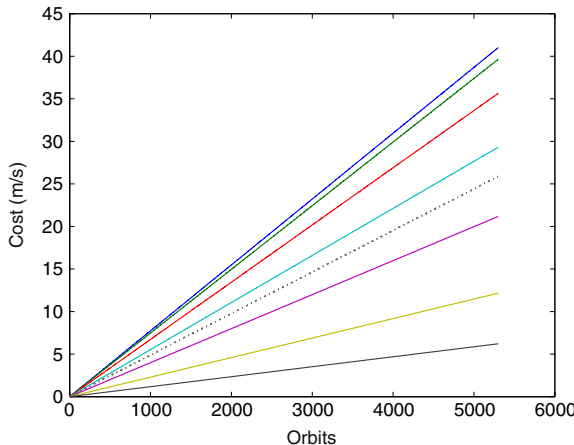


FIGURE 10.19 Formation impulse requirements vs. time with and without fuel balancing for seven satellites with α_0 uniformly distributed between 0° and 180° . Dotted and solid lines indicate impulse magnitudes with and without fuel balancing, respectively.

error from that for the case with $\dot{\alpha} = 0$ is that $\alpha(0)$ is no longer a constant and hence the secular drift rates of the satellites vary with time.

Figure 10.19 shows the variations in the costs for the satellites in the formation with and without fuel balancing. Each solid line in this figure shows the cost for a single satellite, with $\dot{\alpha} = 0$. The lowest cost of 6 m/s/year is that for the satellite with $\alpha(0) = 90^\circ$, which is slightly higher than the 5 m/s/year figure predicted by Eq. (10.54a). The highest cost of 41 m/s/year is incurred by the satellite with $\alpha(0) = 0^\circ$. The result for this case matches perfectly with its analytical estimate, since the out-of-plane cost dominates the total cost. The dotted line in Fig. 10.19 shows the effect of fuel balancing; it is in fact a superposition of seven lines, one for each satellite. The average cost per satellite under the action of the fuel balancing control is 25.8 m/s/year . The total cost for formation maintenance without fuel balancing is 185 m/s/year as compared to 181 m/s/year , obtained with fuel balancing. A decrease, albeit small, in the total cost has been achieved, in addition to the main goal of homogenization of the inter-satellite fuel requirements.

The final set of results pertains to formation maintenances by the application of the two-impulse control scheme during every 10th orbit of the chief. The results for $\alpha(0) = 0$ and $\dot{\alpha} = 0$ are considered first. As can be seen from Fig. 10.20 and Fig. 10.13, the excursions away from the reference PCO are more pronounced when the impulses are applied during every tenth orbit. Notice also that the extreme deviations occur at four locations; these are functions of $\alpha(0)$ of the two-impulse scheme. Figure 10.21 shows that the variation of the error in the radius of the controlled PCO remains bounded within $\pm 41 \text{ m}$. The secular growth is eliminated periodically by the control. The impulse

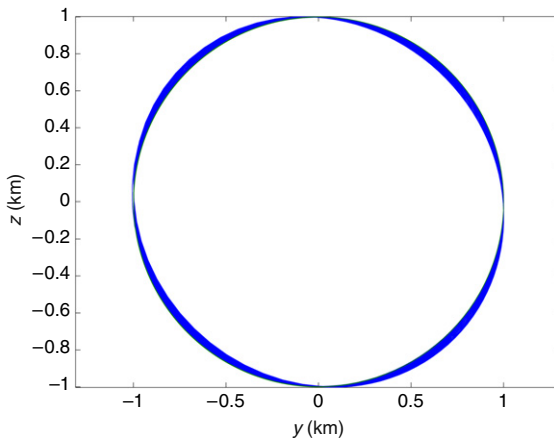


FIGURE 10.20 PCO resulting from the two-impulse control scheme applied during every tenth orbit of the chief, $\alpha(0) = 0$ and $\dot{\alpha} = 0$ (1-year simulation).

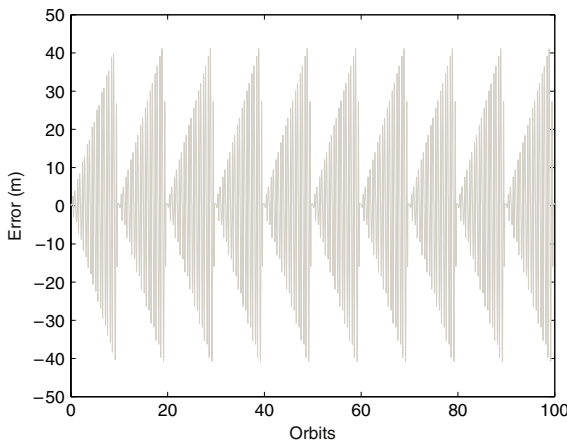


FIGURE 10.21 Evolution of the error in the radius of the PCO for $\alpha(0) = 0$ with control applied during every tenth orbit of the chief, $\dot{\alpha} = 0$ (100 orbits shown).

requirements are shown in Fig. 10.22 for a 100-orbit segment of time. The circles and the stars in this figure indicate, respectively, the magnitudes of the first and second impulses. A comparison of Fig. 10.22 and Fig. 10.14 shows that the impulse magnitudes have been scaled by a factor of 10 for the relaxed mode of operation. However, the total cost for this case is still approximately 41 m/s/year, unchanged from the corresponding case of control applied during every orbit. Delaying impulse application to a time when the orbit error is sufficiently large results in practically realizable thrust levels but it does not

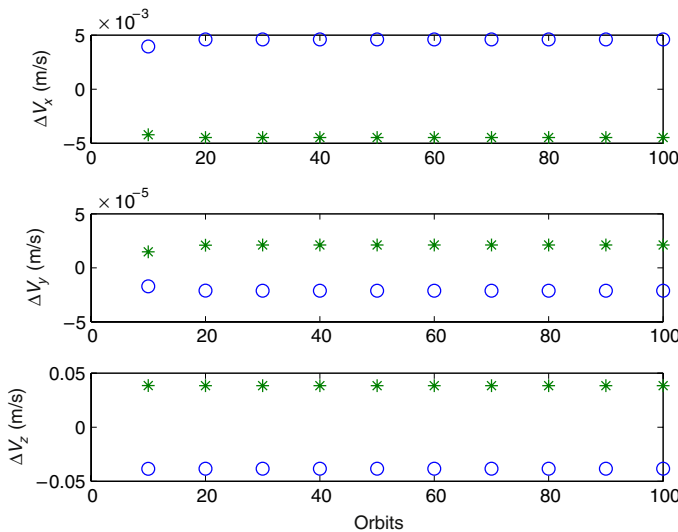


FIGURE 10.22 Impulse components for $\alpha(0) = 0$ and $\dot{\alpha} = 0$, two-impulse control applied during every tenth orbit of the chief, 100 orbits shown.

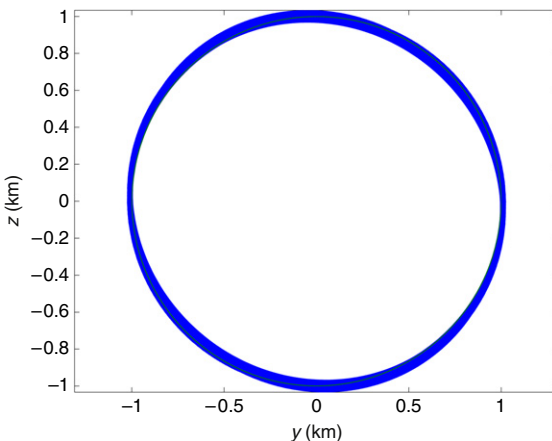


FIGURE 10.23 PCO resulting from the application of the two-impulse control scheme during every tenth orbit of the chief, $\alpha(0) = 0$ and $\dot{\alpha} = -2.723^\circ/\text{day}$ (1-year simulation).

save fuel because a secular perturbation is being dealt with. Figure 10.23 shows the relative orbits for $\alpha(0) = 0$ and $\dot{\alpha} = -2.723^\circ/\text{day}$. It is seen that the resulting levels of excursions away from the reference are higher than those observed in Fig. 10.20. Figure 10.24 shows that the error in the radius of the PCO is bounded by ± 49 m. A longer-horizon trace of the error is shown in Fig. 10.25, which indicates a stable, limit cycle behavior.

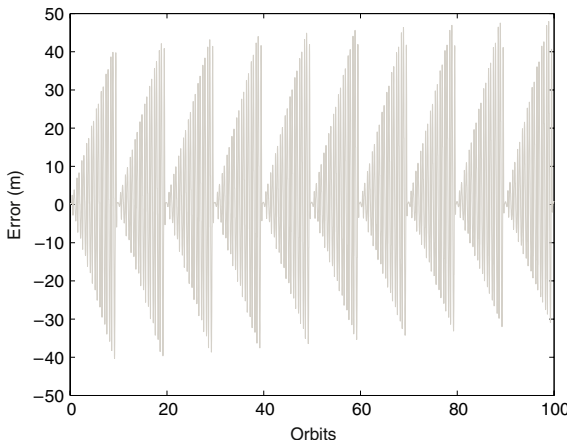


FIGURE 10.24 Evolution of the error in the radius of the PCO for $\alpha(0) = 0$ with control applied during every tenth orbit of the chief, $\dot{\alpha} = -2.723^\circ/\text{day}$ (100 orbits shown).

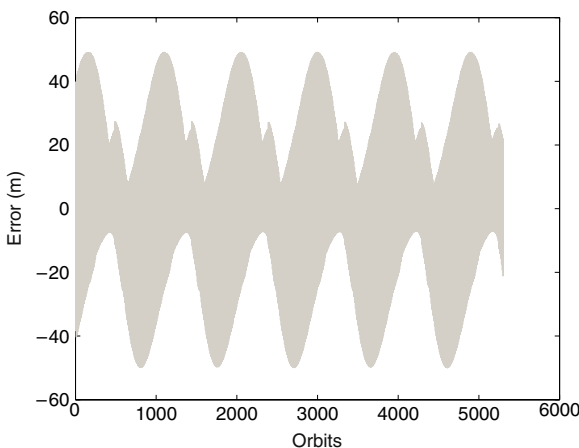


FIGURE 10.25 Evolution of the error in the radius of the PCO for $\alpha(0) = 0$ with control applied during every tenth orbit of the chief, $\dot{\alpha} = -2.723^\circ/\text{day}$ (1-year simulation).

SUMMARY

This chapter presented an overview of various control methods – continuous and discrete for formation establishment, maintenance, reconfiguration, and fuel balancing. Examples of the applications of the CLF and LQR methods were presented in conjunction with the feedback of errors based on mean and averaged elements. The application of an optimization technique for computing multi-impulse reconfiguration maneuvers was presented. Radial component of the thrust was inhibited for the example problems for which the formation can be controlled with tangential and cross-track controls. Application of the open-loop optimal multi-impulse maneuver strategy is impractical for

long-duration formation maintenance problems. Hence, a simple two-impulse-per-orbit scheme was also treated for which the impulses can be calculated analytically, effectively producing a feedback control approach. In all the cases presented, the benefit of controlling the mean rather than the osculating orbital elements was highlighted. Furthermore, many of the theoretical estimates for thrust or impulse magnitudes derived in the previous chapters were shown to be achievable under ideal control application to the nonlinear equations of motion. Simulations with higher-fidelity models and the effects of noise or the results of using estimated states were not treated in this chapter. These topics are addressed in the following chapters.